Understanding the Long-term Trend of Organic Aerosol and the Influences from Anthropogenic Emission and Regional Climate Change in China

Wenxin Zhang[1], Yaman Liu[1,2], Man Yue[1,2], Xinyi Dong[1,3,4], Minghuai Wang[1,4]

[1]School of Atmospheric Science, Nanjing University, Nanjing, 210023, China
[2]Zhejiang Institute of Meteorological Sciences, Hangzhou, 310008, China
[3]Frontiers Science Center for Critical Earth Material Cycling, Nanjing University
[4]Joint International Research Laboratory of Atmospheric and Earth System Sciences & Institute for Climate and Global Change Research, Nanjing University, Nanjing, 210023, China

Correspondence to: Xinyi Dong (dongxy@nju.edu.cn)

Abstract. Organic aerosol (OA) is a major type of fine particulate matter. OA shows a large variability influenced by anthropogenic emissions, vegetation, and meteorological changes. Understanding OA trends is crucial for air quality and climate studies, yet changes in OA over time in China are poorly documented. This study applied the Community Atmosphere Model version 6 with comprehensive tropospheric and stratospheric chemistry (CAM6-Chem) to investigate long-term OA trends in China from 1990 to 2019 and identify the driving factors. The simulations agreed well with ground-based measurements of OA from 151 observational sites and the CAQRA reanalysis dataset. Although OA trends showed a modest 5.6% increase, this resulted from a significant -8.1% decrease in primary organic aerosols (POA) and a substantial 32.3% increase in secondary organic aerosols (SOA). Anthropogenic emissions of POA and volatile organic compounds (VOCs) were the dominant contributors to these trends. While biogenic VOCs (BVOCs) played a secondary role in SOA formation, significant changes were observed in specific sub-species: isoprene-derived SOA decreased by -18.8% due to anthropogenic sulfate reduction, while monoterpene-derived SOA increased by 12.3% driven by enhanced emissions from rising temperatures. Our study found through sensitivity experiments a negligible response of monoterpene-derived SOA to changes in anthropogenic nitrogen oxides (NOx) emissions as a net effect of changes in multiple pathways. This study highlights the complex interplay between POA reduction and SOA growth, revealing notable OA trends in China and the varying roles of both anthropogenic and biogenic emissions.

1. Introduction

$PM_{2.5}$ (particulate matter less than or equal to 2.5 micrometers in diameter) is a standard air pollutant and attracts numerous research attention during the past decade. Ground level mass concentration of $PM_{2.5}$ was found to gradually increase during 2000-2013 and then decreased since 2014 in China (An et al., 2019; Lin et al., 2018; Ma et al., 2016). The trend of $PM_{2.5}$ is believed to be driven primarily by China's emission control policies (Lu et al., 2020; Tong et al., 2020) and regional climate

change over East Asia, which affects the dispersion condition (Xu et al., 2022). Organic aerosol (OA) is an important component of PM$_{2.5}$ as it can contribute up to 77% of total fine mode particles during haze pollution episode (An et al., 2019; Zhong et al., 2021). Despite its significance, there have been limited studies involving long-term continuous observations of OA. Unlike PM$_{2.5}$, the observational gaps restrict our understanding of historical trends in OA, making it challenging to access

35   air quality changes accurately and formulate effective environmental policies. While a few existing modeling studies have explored recent changes in OA in China, they often cover only limited time periods or specific years (Chen et al., 2024a; Zheng et al., 2023b).

OA consists of primary organic aerosols (POA) and secondary organic aerosols (SOA). POA is largely emitted from

40   anthropogenic sources such as vehicle emissions, residential biofuel usage, and industrial activities, as well as biomass burning. Consequently, POA emissions are usually intensive (Fadel et al., 2021; Kanellopoulos et al., 2021) in urban areas (Liu et al., 2023) with their impact being primarily localized due to dependence on anthropogenic sources. Control of POA emissions has been effective in reducing PM$_{2.5}$ concentrations, as observed in regions like the Western United States (Pye et al., 2019). In China, studies have also reported a significant contribution of POA to PM$_{2.5}$. Huang et al. (2019) discovered that POA emerges

45   as the primary constituent during pollution episodes in the North China Plain (NCP) region (Huang et al., 2019). Zheng et al. (2023a) found a decrease of 11.8 μg m^{-3} in OA concentrations at Beijing over 2005-2018, with most of the decrease coming from POA.

On the other hand, SOA is mainly produced through complex transformations of volatile organic compounds (VOCs) emitted

50   from both anthropogenic and biogenic sources (Hallquist et al., 2009; Qin et al., 2018; Shrivastava et al., 2017; Zhang et al., 2007). These VOCs undergo multiple oxidation processes in the atmosphere, making SOA formation sensitive to chemical reactions, as well as meteorological conditions (An et al., 2019; Fan et al., 2020; Hu et al., 2017). In Southern China, biogenic VOCs (BVOCs), primarily monoterpenes and isoprene, are significant contributors to SOA formation, particularly during summer due to warm temperatures and extensive vegetation (Guenther et al., 2012). Given that SOA formation is affected by

55   both anthropogenic and natural factors, the response of OA to changing emission and climate conditions is likely nonlinear.

In the context of global warming, China has made considerable efforts to reduce anthropogenic emissions through a range of climate policies (Cai et al., 2017; Cui et al., 2020; Feng et al., 2019; Zheng et al., 2018). These measures have led to reductions in both POA and SOA concentrations. However, biogenic SOA (BSOA) also plays an important role in determining OA trends

60   as it may change due to anthropogenic emission change. For example, studies indicate that BSOA produced from isoprene-epoxydiols (IEPOX) has significantly decreased in the Southeast United States due to reductions in anthropogenic SO$_2$ emissions (Hoyle et al., 2011; Liu et al., 2021b; Qin et al., 2018; Shilling et al., 2013; Shrivastava et al., 2019), and a similar response was also reported in China (Dong et al., 2022). Likewise, monoterpene-derived SOA (SOA$_{MT}$) is sensitive to nitrogen

oxides (NOx) concentrations, and interactions between NOx and BVOCs can alter the oxidation pathways and ultimately affect BSOA formation (Jo et al., 2019; Xu et al., 2021; Zhang et al., 2018).

The abovementioned studies suggest that the long-term trends in OA might be a net result of the opposing trends in its sub-species, driven by multiple anthropogenic and natural factors. Nevertheless, existing modeling studies largely attribute OA trends to emission changes without detailed consideration of different sub-species. Moreover, the interactions between BVOCs and changing climate conditions complicate predictions of BSOA responses, hindering accurate forecasts of future OA trends. Diagnostically investigating OA trends and driving factors is therefore crucial to ensure a more comprehensive assessment of air quality changes. Given the limited availability of long-term observational data, this study employs a modeling tool along with available observation and reanalysis dataset to explore the long-term trends of OA in China from 1990 to 2019, considering contributions from different sub-species. This analysis aims to support future air pollution control strategies by providing a better understanding of OA and its driving factors, thereby enabling more effective management of air quality in the face of ongoing climate change.

2. Data and Methods

2.1 Model Configuration

This study uses the Community Atmospheric Model version 6 with comprehensive tropospheric and stratospheric chemistry (CAM6-Chem) from the Community Earth System Model version 2.1.0 (CESM2.1.0). The gas-phase chemistry is represented by the Model for Ozone and Related chemical Tracers (MOZART) chemical mechanism (MOZART-TS2) including comprehensive isoprene and monoterpenes chemistry (Schwantes et al., 2020). The aerosol model utilizes the four-mode version of the Modal Aerosol Module (MAM4) (Liu et al., 2016) and employs the Volatility Basis Set (VBS) approach (Donahue et al., 2006; Hodzic et al., 2016) to simulate SOA formation. VOCs (isoprene, glyoxal, monoterpenes, sesquiterpene, benzene, toluene, lumped xylenes, intermediate volatile organic compounds and semi-volatile organic compounds) are oxidized to produce five different types of volatile SOA gaseous precursors, with volatilities corresponding to effective saturation concentrations (C*) of 0.01, 0.1, 1.0, 10.0, and 100.0 μg/m^3 at 300 K, respectively (Tilmes et al., 2019). Heterogeneous production of isoprene-epoxydiol-derived SOA (SOA$_{IE}$) is represented within the coupled Model for Simulating Aerosol Interactions and Chemistry (MOSAIC) (Jo et al., 2019, 2021; Zaveri et al., 2008, 2021) mechanism. The photolysis rate of monoterpene-derived SOA is updated based on our previous work (Liu et al., 2023). Aerosol wet removal scheme uses the Cloud Layers Unified By Binormals (CLUBB) scheme to unify shallow convective and stratiform clouds, coupled with the two-moment cloud microphysics scheme by Gettelman and Morrison (2015) (MG2) for aerosol activation and removal (Gettelman and Morrison, 2015). For deep convective clouds, the scheme employs the parameterization by Zhang

and McFarlane (1995) (ZM95) and relies on empirical parameters for estimating aerosol wet removal processes (Zhang and
95   McFarlane, 1995).

We conducted long-term simulations covering the period from 1990 to 2019. The horizontal resolution of the simulations is
set to 0.95° for latitude and 1.25° for longitude, with 32 vertical layers extending to approximately 40 kilometers. The
simulation has a spin-up time of 1 year and a relaxation time of 50 hours to investigate surface OA trends. Natural emissions
100   are calculated online using the Model of Emissions of Gases and Aerosol from Nature version 2.1 (MEGAN2.1), which is
coupled to the CESM model (Emmons et al., 2020; Guenther et al., 2012). Anthropogenic emissions from 1990 to 2019 were
sourced from the multi-resolution emission inventory for China (MEIC, http://www.meicmodel.org) (Li et al., 2017).
Intermediate volatile organic compounds (IVOC) and Semi-volatile organic compounds (SVOC) emissions were scaled
based on POA emissions and non-methane VOC emissions (Chang et al., 2022; Tilmes et al., 2019), with specific formulas
105   provided in the supplement. We used the Modern-Era Retrospective analysis for Research and Applications (MERRA2)
reanalysis data (Gelaro et al., 2017) for meteorological constraints.

To distinguish the effects of biogenic emissions and anthropogenic NOx emissions on SOA$_{MT}$, we conducted additional
sensitivity simulations by applying scaling factors for monoterpenes and NOx emissions respectively. Monoterpenes emissions
110   are higher in summer (Zhang et al., 2018), and 2013 saw the peak monoterpenes emissions (Fig. 8(a)), while NOx
concentrations reached a secondary peak (Fig. 8(b)). Therefore, we have selected July 2013 for sensitivity simulations to better
capture SOA$_{MT}$'s response to both emission types. A benchmark simulation was conducted and denoted as 100nudging, which
has the same configuration as the long-term simulation but with a 0.5-hour relaxation time to minimize the impact of
meteorological fields (Liu et al., 2021a; Tilmes et al., 2019). One type of sensitivity experiment was monoterpenes emission
115   experiments, and the two sets of experiments were named 0.5MTERP and 2MTERP. Their model configurations were the
same as those of 100nudging, but the monoterpenes emissions were respectively set to 0.5 and 2 times the 100nudging
emissions. Their differences relative to 100nudging indicated the impact of monoterpenes emissions disturbance on SOA$_{MT}$
formation. The other type of sensitivity experiment was NOx emission experiments, and the two sets of experiments were
named 0.5NOx and 2NOx. Their model configurations were also the same as those of 100nudging, but the NOx emissions
120   were respectively set to 0.5 and 2 times the 100nudging emissions. Their differences relative to 100nudging indicated the
impact of NOx emissions disturbance on SOA$_{MT}$ formation.

The model used in this study classifies monoterpenes into four categories: α-pinene, β-pinene, limonene, and myrcene. In the
following sections, these will be collectively referred to as monoterpenes. In this study we constrained BSOA as the summary
125   of SOA$_{MT}$ and SOA$_{IE}$ to focus on these two most important contributors. It shall be mentioned that isoprene and monoterpenes

make the most contribution to BVOCs in China (Ding et al., 2016). Therefore, this study specifically focuses on the impact of aerosols derived from these compounds on OA trends.

2.2 Observations

We used observations from a number of different sources to evaluate the simulation performance of major aerosol species as
130 well as key intermediates. We used ground-based measurements compiled by Miao et al. (2021) and Chen et al. (2024), which provided mean mass concentrations of surface OA, POA, and SOA in China from 2013 to 2019, along with the corresponding station locations (Chen et al., 2024a; Miao et al., 2021). A total of 151 measurements were included by removing duplicate values. We also used the high-resolution simulation dataset of $PM_{2.5}$ composition over China (CAQRA-aerosols) provided by the National Natural Science Foundation Air Pollution Complex Major Research Plan Data Integration Project (Project
135 Number: 92044303, https://www.capdatabase.cn). The CAQRA-aerosols data were developed using emission inversion and high-resolution numerical simulation techniques (Kong et al., 2021). The CAQRA-aerosols data provided mass concentrations of organic carbon (OC) rather than OA (Kong et al., 2021). The root mean square error of OC on the monthly average concentration scale was 12.0 μg/m³, with a mean bias of 0.03 μg/m³ (0.17%) (Kong et al., 2021). We used OA/OC ratios (1.19-3.04) to convert OC to OA concentrations (Malm and Hand, 2007) to facilitate comparison with simulation results. Since ratios
140 vary with site and season, we used the mean value of 1.8 recommended by Malm and Hand (2007) as the conversion factor (Malm and Hand, 2007). To understand the model performance for simulating air pollutants, we also analyzed them by comparing them with the output values at the corresponding times and locations in the model. The 24h average $PM_{2.5}$ and ozone (O_3) data from the China Environmental Monitoring Terminal (CEMT) National Urban Air Quality Real-Time Distribution Platform (NUAQRDP) (https://air.cnemc.cn:18007/) were used to analyze changes in surface aerosol
145 concentrations over the period 2014-2019.

Moreover, we used MODIS Level3 Collection 6.1 monthly aerosol optical depth (AOD) data as an indicator for column density of fine size aerosols. The 550 nm AOD data were retrieved using the combined Dark Target-Deep Blue algorithm (Levy et al., 2013), with monthly averaged data covering the years 2000-2019 at a spatial resolution of 1°. Performance of NOx simulation
150 was also assessed using nitrogen dioxide (NO_2) column concentrations monitored by the OMI (Ozone Monitoring Instrument) Level-3 on board NASA's AURA satellite (https://disc.gsfc.nasa.gov/datasets?keywords=OMI&page=1), with daily averaged data covering the period 2000-2019 at a spatial resolution of 0.25˚.

3. Results and Discussions

3.1 Evaluation of Model Performance

155 Performance of the model was evaluated by comparing simulation results with ground-based observations, the CAQRA-aerosols dataset and satellite products mentioned in Section 2. The results of the baseline simulation were compared with observations from multiple sources. Overall, the model can generally reproduce the spatial distributions and mass concentrations of OA and its components (Fig.S1). By validation with observations from Miao et al. (2021) and Chen et al. (2024), the modelled normalized mean bias (NMB) of surface OA, POA, and SOA were -34.5%, -7.4%, and -64.8%,

160 respectively. Although there was a general underestimation of surface OA by the model, the simulations showed close agreement with measurements, with a coefficient of determination (R^2) by 0.8. The capability of CAM-Chem in simulating OA over China was generally well consistent with other modeling studies. For example, Qin et al. (2018) utilized the Community Multiscale Air Quality (CMAQ) model (v5.0.2) to evaluate BSOA and reported an NMB of -70% (Qin et al., 2018); Zheng et al. (2023b) employed the Weather Research and Forecasting model (WRF, v3.9)−CMAQ/2D-VBS modeling

165 system and observed an NMB of -20% for POA (Zheng et al., 2023b).

Our model simulated spatial distribution of OA was in good agreement with the CAQRA-aerosols dataset. Both our model and the dataset indicated relatively higher OA concentrations in Eastern China and lower concentrations in Western China (Fig.S2). The CAQRA-aerosols dataset showed that OA has strong seasonality in China, with the highest average mass

170 concentrations in winter and the lowest in summer. Our model simulations reproduced this seasonal characteristic well (Fig.S3). The results of both the model and the CAQRA-aerosols dataset indicated a decreasing trend in OA concentrations in China (Fig.1(b)). Notably, there was good spatial consistency, with a significant decrease observed in Eastern China, particularly in the NCP region (Fig.1(c,f)). This decreasing trend was especially pronounced in Beijing. Given that only the Beijing site had continuous ground-based observations over multiple years from Miao et al. (2021) and Chen et al. (2024), we further evaluated

175 the long-term simulation results for this site. The simulation values showed good agreement with the observed values, reflecting a consistent trend over the years (Fig.1(e)).

In terms of $PM_{2.5}$ simulation, the model slightly underestimated observation by -19.2% (Fig.S6(a)). This might be at least partially because of coarse model grid resolution while CEMT observational sites are mostly within urban area. We then

180 compared the simulation with observation for the contribution of OA to $PM_{2.5}$, showing good performance with an NMB of 5.6%. Observed $OA/PM_{2.5}$ ratio was calculated by paring OA measurements reported in Miao et al. (2021) and Chen et al. (2024) with CEMT $PM_{2.5}$ observations during the same period, which fall into the same CAM6-Chem model grid. Due to lack of synergic collected observations of aerosol subspecies, we didn't validate the contributions from other subspecies but focus on OA only. The moderate underestimations of OA and $PM_{2.5}$ but relatively better performance for simulating $OA/PM_{2.5}$ ratio

185 suggested that although the model may have deficiencies to reproduce the absolute concentrations of OA, it was able to capture

the contribution from OA correctly. It also implied that there might be systematic bias within the modeling system affecting underestimations of aerosol mass concentrations such as coarse grid resolution. Our recent study thoroughly evaluated CAM-Chem simulation of PM$_{2.5}$ in China and reported that a finer grid (~0.25°) would substantially lower modeling bias, especially over complex terrains during haze episodes (Yue et al., 2023). The fine grid version was not employed in this study as it's not
190   compatible with MOSAIC module yet, and we consider the heterogeneous chemistry of SOA and thermodynamic equilibrium of nitrate represented by MOSAIC is more important for this study to focus on long-term trend of OA and subspecies.
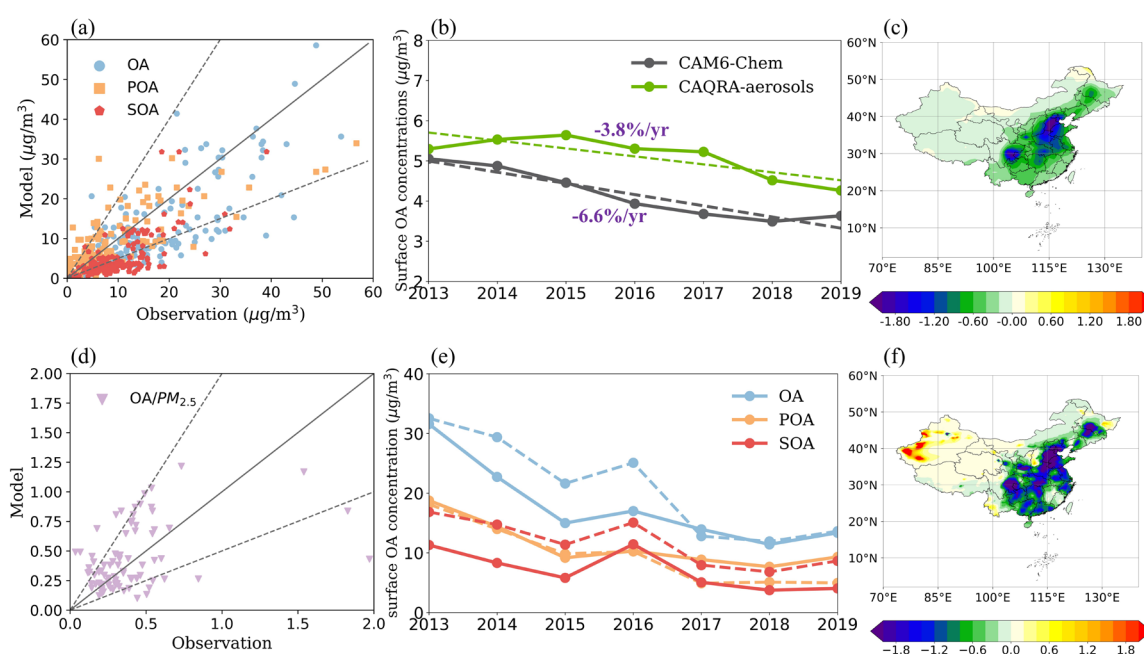
Figure 1: (a) Validation of modelled organic aerosols (OA), primary organic aerosols (POA), and secondary organic aerosols (SOA)
195   **based on ground-based measurements compiled by Miao et al. (2021) and Chen et al. (2024) (unit: µg m⁻³). (b) 2013 to 2019**
interannual variation of average surface organic aerosol (OA) concentrations in CAM6-Chem (dark grey) and the CAQRA-aerosols
dataset (green) (unit: µg m⁻³) and their trend lines (dotted line). (c) 2013 to 2019 CAM6-Chem modelled annual long-term trend of
surface OA concentrations (unit: µg m⁻³ per year). The trend is calculated by linear regression on an annual scale over 1990-2019.
(d) Validation of modelled OA/PM$_{2.5}$ based on OA measurements compiled by Miao et al. (2021) and Chen et al. (2024) and PM$_{2.5}$
200   **observations from the National Urban Air Quality Real-time Release Platform of China Environmental Monitoring Station. (e)**
Interannual variation of average surface OA, POA and SOA concentrations (µg m⁻³) at Beijing site from 2013 to 2019 in CAM6-
Chem (solid line) and ground-based measurements compiled by Miao et al. (2021) and Chen et al. (2024) (dashed line). (f) 2013 to
2019 annual long-term trend of surface OA concentrations (unit: µg m⁻³ per year) in the CAQRA-aerosols dataset. The trend is
calculated by linear regression on an annual scale over 1990-2019.

205   **3.2 Trend and attribution of Surface OA**

In this section we first briefly introduced the general characteristics (e.g., concentrations, main sub-species, spatial distribution) of simulated OA, and then investigated the overall change of OA through the study period.

Spatial distributions of annual average concentrations of OA and related subspecies are presented in Fig.2. The concentrations
210 of OA show prominent regional differences, with its high values (>15 μg m^{-3}) areas concentrated in the NCP and Sichuan
Basin Area (SBA), while the vast remote areas in Western China such as Tibet and Xinjiang show lower OA concentrations
(<5 μg m^{-3}). Spatial distribution of total OA at national scale is predominantly determined by POA as shown in Fig.2(b). In
the densely populated NCP urban area, contribution of POA to OA can reach up to 75%. SOA was relatively lower in
concentration (Fig.2(c)) and was found to have a consistent spatial distribution pattern as POA, indicating a dominate
215 contribution from anthropogenic VOCs derived SOA (ASOA) to total SOA. Spatial distributions of POA and SOA are
generally well consistent with anthropogenic POA and VOCs emissions which also concentrated over urban clusters as shown
in Fig.2(d) and (e) respectively. Pearl River Delta (PRD) is found to be unique as it has relatively low POA emissions but high
anthropogenic VOCs emission, probably due to vehicle exhausts (Lee et al., 2002; Liu et al., 2024). It is also important to
notice that Southern China has a non-negligible level of SOA where biogenically produced BSOA was found to play an
220 important role due to extensive vegetation coverages with excessive BVOCs emissions as shown in Fig.2(f). For example,
contributions of BSOA to OA can reach up to 27% over Yunnan-Guizhou Plateau for climatological summer averages.
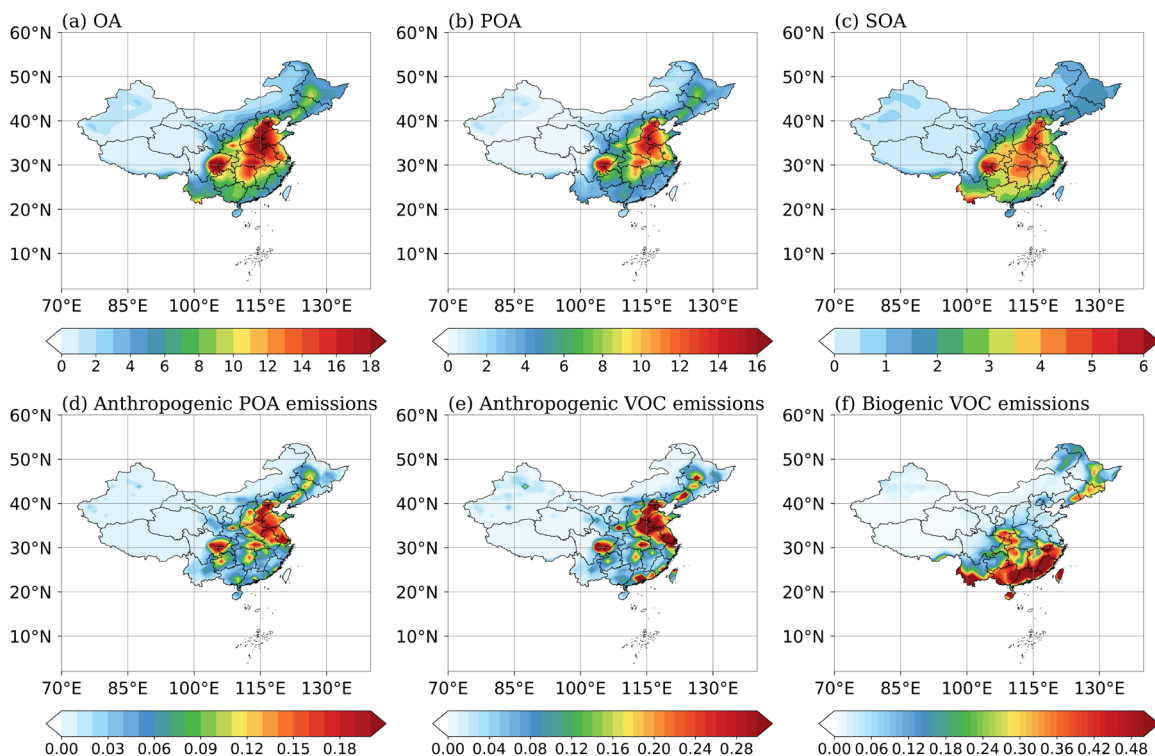
Figure 2: **1990 to 2019 annual average of surface organic aerosols (OA; a; unit: μg m^{-3}), primary organic aerosols (POA; b; unit:**
225 **μg m^{-3}), secondary organic aerosols (SOA; c; unit: μg m^{-3}). 1990 to 2019 annual average of anthropogenic POA emissions (d; unit:**
g m^{-2} mon^{-1}), anthropogenic volatile organic compounds emissions (e; unit: g m^{-2} mon^{-1}), and biogenic volatile organic compounds
emissions (f; unit: g m^{-2} mon^{-1}) concentrations.

General trends of OA and sub-species were demonstrated in Fig.3, with more details such as time series plots (Fig. S7, S11),
230 trends at seasonal scale (Fig. S14, S15, S17) are presented in supplementary materials. All trends are calculated by linear
regression on annual scale over 1990-2019. In general, trend of surface OA concentrations showed a regional difference as
decreasing over eastern coastal provinces and increasing over the western inland provinces. For example, the annual average
surface OA concentrations showed a significant decreasing trend over Yangtze River Delta (YRD) by around -1.4 μg m^{-3} per
decade (-13.8% per decade). While in SBA, surface OA shows an increasing trend by 0.4 μg m^{-3} per decade (7.3% per decade).
235 Trends in different seasons were consistent with the annual trend mentioned above but with stronger changes, as the increase
of OA over SBA in summer was more prominent, and so did the decrease over YRD in winter (Fig.S14).
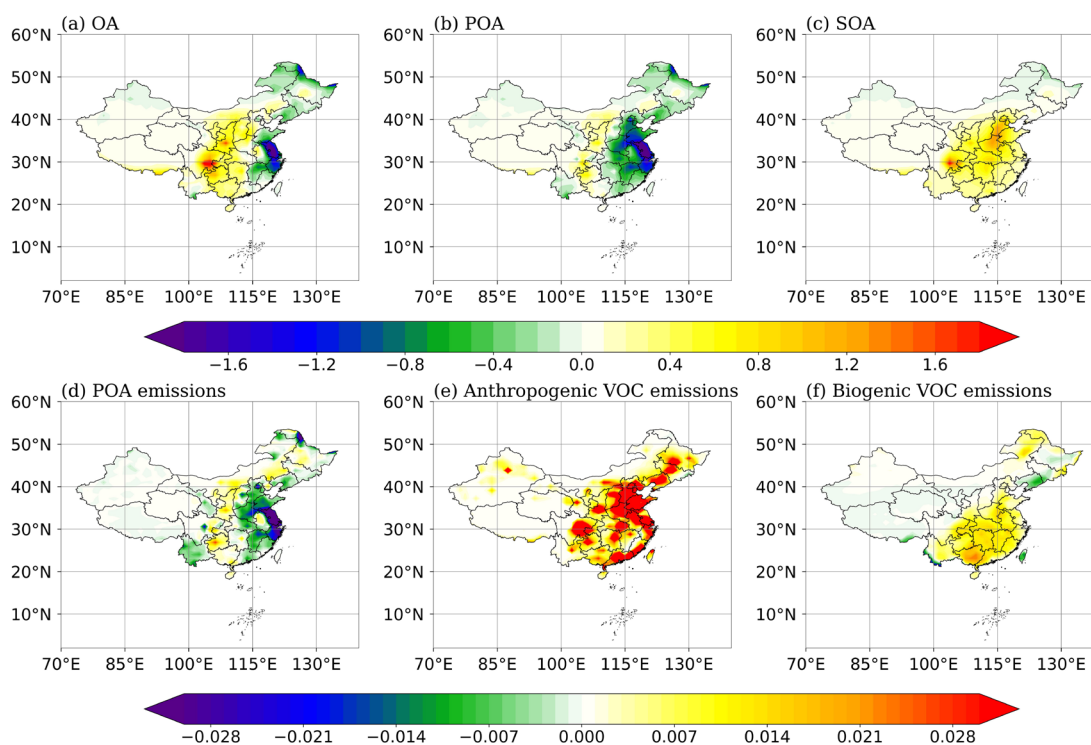
Figure 3: 1990 to 2019 annual average long-term trend of surface organic aerosols (OA; a; unit: μg m^{-3} per decade), primary organic
240 **aerosols (POA; b; unit: μg m^{-3} per decade), secondary organic aerosols (SOA; c; unit: μg m^{-3} per decade), primary organic aerosols**
emissions (d; unit: g m^{-2} per decade), anthropogenic volatile organic compounds emissions (e; unit: g m^{-2} per decade), biogenic
volatile organic compounds emissions (f; unit: g m^{-2} per decade).

The overall OA trend is the net result of the long-term changes in its sub-species POA (Fig. 3(b)) and SOA (Fig. 3(c)). POA
245 generally showed consistent trends with total OA which decreased in the east by up to -8.9% per decade (-0.24 μg m^{-3} per
decade) and increased in the west by up to 13.2% per decade (0.08 μg m^{-3} per decade). SOA showed a clear upward trend

throughout the country by 10.8% per decade (0.16 µg m⁻³ per decade). The spatial distributions of the long-term trends of POA and SOA were well consistent with the pattern of changes in emissions as shown in Fig.3(d-f).

250 It's interesting to notice that the most significant changes in OA were not over the regions with high OA concentrations. The different patterns of changes in POA and SOA lead to various changes of OA over three typical urban cluster areas including NCP, YRD, and SBA. NCP has the highest level of total OA but a minor trend, probably due to the net effect of a minor decrease in POA and an increase in ASOA, both driven by changes in anthropogenic emissions. YRD has the lowest level of total OA concentration but the most significant decreasing trend, primarily due to the reduction of POA. Zheng et al. (2023a)

255 suggested that anthropogenic POA emissions were reduced by -65.7% in YRD over 2005-2019 as a result of air quality management (Zheng et al., 2023b). SBA has a relatively high level of OA and also the most significant increasing trend. Changes in emissions suggested that the enhancement was mainly driven by excessive SOA from anthropogenic precursors, as shown in Fig.3(e). A more detailed discussion of anthropogenic and biogenic contributions to this increased SOA over SBA will be provided in later sections.

260
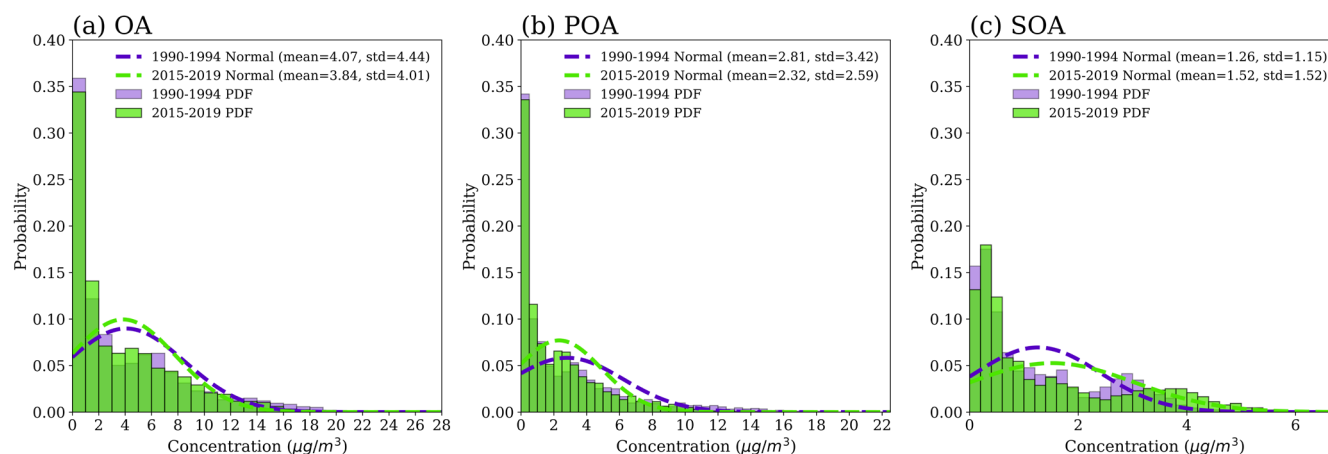
Figure 4: The probability density function (PDF) distributions of the simulated five-year average concentrations of OA (a), POA (b), and SOA (c) for the periods 1990-1994 (purple) and 2015-2019 (green). The dashed lines represent the normal distributions fitted based on the calculated mean and standard deviation. The calculated mean and standard deviation are also displayed in the figures.

265

Given China's vast area, we used probability density function (PDF) to analyze the distribution of OA and its components across different concentration ranges for all grid points, complementing the overall trend analysis. Fig.4(c) shows that the PDF for SOA concentrations shifted right, with higher probability density values, leading to a significant national increase in SOA levels. In contrast, POA trends moved in the opposite direction (Fig.4(b)). While Western China's vast area may impact

270 arithmetic averages, PDF analysis still shows a significant rise in SOA levels, which is consistent with the annual variations

calculated using arithmetic averages. To better understand the impact of low OA concentration areas like Xinjiang, Tibet, and Qinghai (Fig.2 (a)), we also analyzed trends while excluding these regions (Table S2). The calculated trends indicate that the impact of low concentration regions is limited, while the overall trend is dominated by changes in high concentration areas.

3.2.1 Attribution of POA trend

275 We analyzed the decreasing trend of POA and found that both anthropogenic emissions and biomass burning were responsible for it. Anthropogenic emissions contributed 87.4% and dominated the long-term trend, while biomass burning substantially affected the inter-annual variation (IAV) although it only contributed by 12.5% emission on average. As shown in Fig.5(a) and Fig.S7(a), variations in biomass burning are responsible for the large IAV of POA concentrations. Biomass burning usually has a strong seasonality, so we analyzed its contribution across different seasons (Fig.5(b)). We found that biomass burning in

280 China was most intensive in spring as the relative contribution to total POA emission was 21.4%. Previous studies have also reported the significant contributions from biomass burning in China, mainly due to agricultural activities. For example, extreme crop residue burning events occurred in Northeast China and Northwest China in 2003 which greatly deteriorated air quality (Wang et al., 2020; Zhuang et al., 2018).

285 As the largest source of POA, anthropogenic emissions of POA decreased by -7.8% from 1990 to 2019 and is in good agreement with the change of POA concentration. As mentioned in Section 3.3, the change in POA concentration was non-monotonic, which can be explained by the varied changes in anthropogenic POA emissions, as shown in Fig. 5(a). Anthropogenic POA emissions were primarily from residential usage of coal and biofuel (78%), followed by a minor contribution from industry (18%) (Zheng et al., 2018). It increased by 1.6% per year over 1990-2006 along with the expansion

290 of population and Gross Domestic Product (GDP) (Liu et al., 2022; Xing et al., 2022), and then started to gradually decrease by -1.7% per year over 2006-2013 as a result of the emission control policies for industrial sources such as manufacturing boilers (Zheng et al., 2018). Since 2014, China has started to strictly implemented more efficient and national emission control policies which greatly lower the anthropogenic emission. Policies such as "Action Plan for Air Pollution Prevention and Control" have been reported to play a pivotal role in emission reduction by imposing restrictions on coal use and implementing

295 advanced emission control technologies (Cai et al., 2017; Cui et al., 2020; Feng et al., 2019; Maji et al., 2020). As a result, a rapid reduction of anthropogenic POA emission started from 2014, which is attributed to broadly replace residential usage of coal and biofuel with electricity and gas. These policies significantly lower the total POA emission by -42.8% over 2014-2019 (Zheng et al., 2018). Since residential POA emission was mainly for cooking and heating purposes, we also analyzed the seasonality of anthropogenic POA emission and found winter indeed showed the greatest contribution (Fig.5(b)). In summary,

300 the changes in POA concentration and POA emissions during the past 30 years in China could be well explained by the implementation of a series of air pollution management activities.
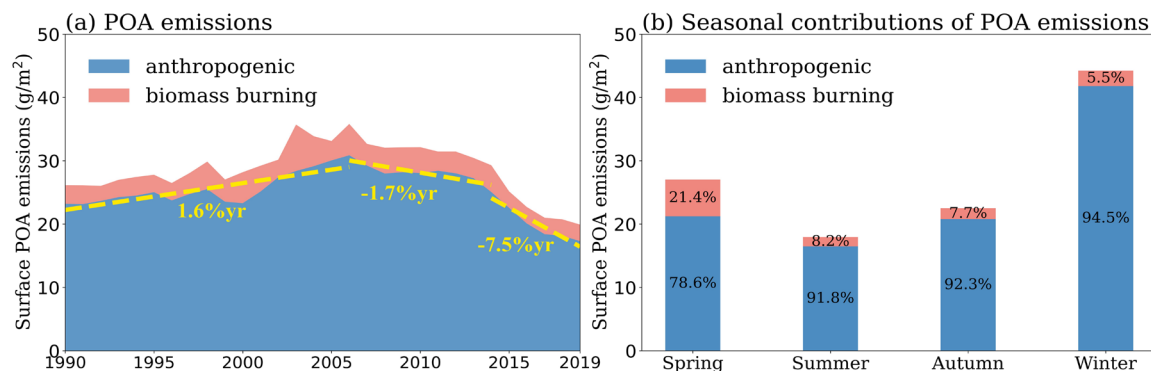
Figure 5: (a) 1990 to 2019 interannual variation of average surface anthropogenic (blue) and biomass burning (pink) primary organic aerosols (POA) emissions (unit: g m⁻² mon⁻¹). The yellow dashed line represents the linear regression fit for anthropogenic POA emissions over the periods 1990–2006, 2006–2014, and 2014–2019. (b) Seasonal average surface anthropogenic (blue) and biomass burning (pink) POA emissions (unit: g m⁻² mon⁻¹) and the relative contribution of different seasons (%).

3.2.2 Attribution of SOA trend

SOA is produced from both anthropogenic and biogenic emissions of VOCs. ASOA contributed roughly 74.3% to total SOA during the study period, with high concentrations found over urban areas such as NCP, YRD, SBA, and PRD. Anthropogenic VOCs mainly consist of aromatics (AVOC), semi-volatile organic compounds (SVOC), and intermediate-volatile organic compounds (IVOC). In contrast to POA, which primarily comes from residential sector, emission sources of anthropogenic VOCs are quite complex and have different changes in China over the past decades. AVOC is mainly emitted from industry (21%), solvent usage (25%), and transportation (22%) (Zheng et al., 2018). Both industry and solvent usage gradually increased over the past decades and subsequently lead to enhanced AVOC emission although transportation slightly decreased. Anthropogenic AVOC increased by 115.8% from 1990 to 2019, with most significant enhancement over urban clusters mentioned above. Although a prominent decrease of AVOC was observed from 2014-2019, it remains the largest contributor of anthropogenic VOCs as shown in Fig.6(b). SVOC are mainly emitted from the same sources as POA (Chang et al., 2022), which also gradually increased before 2006 but decreased since then. IVOC increased throughout the study period but the relative contribution to total anthropogenic VOCs emission was minor. A pilot study suggested that S/IVOC might be the main source of SOA in urban areas (Zheng et al., 2023c).
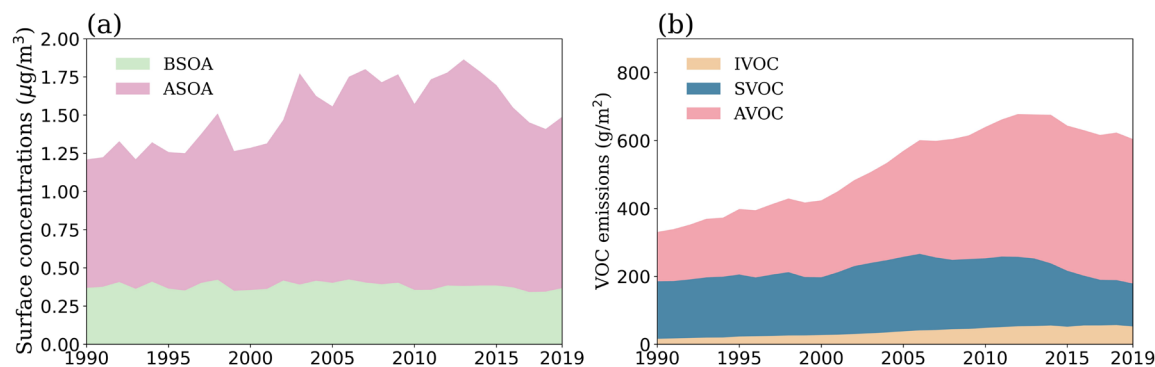
Figure 6: (a) Interannual variations in modelled average surface concentrations of secondary organic aerosols from anthropogenic sources (ASOA) and biogenic sources (BSOA) (unit: μg m⁻³). (b) Interannual variations in emissions of aromatics (AVOC), semi-volatile organic compounds (SVOC), and intermediate-volatile organic compounds (IVOC) (unit: g m⁻² mon⁻¹).

BSOA was found to play an important role especially during summer over South China, and recent studies also revealed that formation of BSOA is closely affected by anthropogenic pollutants such as sulfate and NOx (Liu et al., 2021b; Pye et al., 2013). To understand the contribution of BSOA to the long-term trend of total OA over China, we further analyzed the trend of SOA_{IE} and SOA_{MT}, which are the two main components of BSOA. During 1990-2019, SOA_{IE} concentrations decreased by -0.01 μg m⁻³ per decade (-6.3% per decade). The reduction of SOA_{IE} appears to be primarily driven by the combined effect of IEPOX and SO_4^{2-} availability, as the formation mechanism of SOA_{IE} fundamentally relies on the heterogeneous uptake of IEPOX onto sulfate aerosols (Dong et al., 2022; Jo et al., 2019, 2021). On one hand, anthropogenic emission of SO_2 has been greatly lowered by the enforcement of the Energy Conservation and Emission Reduction (ECER) and a corresponding decrease in the concentrations of SO_4^{2-} has been observed (Fig.S16(d)). This is responsible for the decrease in SOA_{IE} since 2006. On the other hand, the precursor IEPOX showed an opposite decreasing trend (Fig.S16(e-f)) as compared to anthropogenic emission enhancement of NOx before 2011, since NOx would affect the oxidation pathway of isoprene. We find a nationwide reduction of SOA_{IE} over the study period, with an exceptional increase in Yunnan province. The increase of SOA_{IE} over Yunnan province shall be due to the combined effect of enhancement in vegetation coverage resulting from ecosystem projects in China (Hua et al., 2018) and the increase of SO_4^{2-} transported from Peninsular Southeast Asia (e.g., Vietnam, Thailand) resulted from development of local industries (Dalsøren et al., 2009; Grandey et al., 2018). In summary, our results suggested that the change in SOA_{IE} is affected by SO_4^{2-}, which is consistent with previous studies using different models (Liu et al., 2021b; Qin et al., 2018).
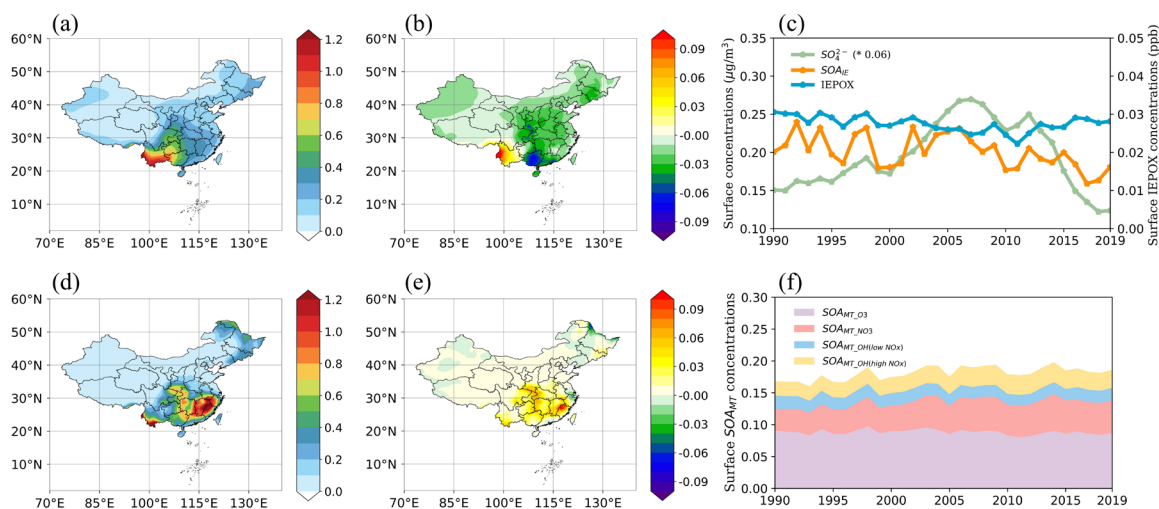
Figure 7: (a) 1990 to 2019 annual average of surface SOA$_{IE}$ (isoprene-epoxydiol-derived secondary organic aerosols; unit: μg m^{-3}) concentrations. (b) 1990 to 2019 annual average long-term trend of surface SOA$_{IE}$ (unit: μg m^{-3} per decade) concentrations. (c) Interannual variations of average surface SOA$_{IE}$ (left Y axis), IEPOX (isoprene epoxydiol; right Y axis) and SO$_4^{2-}$ (scaled by a factor of 0.06; left Y axis) concentrations during 1990-2019. (d) 1990 to 2019 annual average of surface SOA$_{MT}$ (monoterpene-derived secondary organic aerosols; unit: μg m^{-3}) concentrations. (e) 1990 to 2019 annual average long-term trend of surface SOA$_{MT}$ (unit: μg m^{-3} per decade) concentrations. (f) Interannual variations of average surface SOA$_{MT}$ and its subspecies concentrations during 1990-2019 (unit: μg m^{-3}).

Monoterpene-derived SOA was sensitive to both NOx level and biogenic emission, so we first analyzed the trend of SOA$_{MT}$ and its subspecies and then employed sensitivity simulations to distinguish the influences from chemistry and emission. Monoterpenes can be oxidized by different oxidants to form SOA$_{MT}$, so the change in anthropogenic NOx emission may affect the trend of SOA$_{MT}$ by altering the oxidation pathways. We found in the long-term simulation that the net effect of different oxidation pathways led to an overall increasing trend of SOA$_{MT}$, as shown in Fig.7(e-f). We defined four subspecies of SOA$_{MT}$: SOA$_{MT\_O_3}$, SOA$_{MT\_NO_3}$, SOA$_{MT\_OH(low\ NOx)}$, and SOA$_{MT\_OH(high\ NOx)}$, which are produced from O$_3$ oxidation, nitrate radical (NO$_3$) oxidation, hydroxyl radical (OH) oxidation under low NOx condition and OH oxidation under high NOx condition, respectively. The main contributor to SOA$_{MT}$ concentration in China was SOA$_{MT\_O_3}$ (34.6%, Fig.S17(a)), followed by SOA$_{MT\_NO_3}$ (31.2%, Fig.S17(c)), SOA$_{MT\_OH(high\ NOx)}$ (18.1%, Fig.S17(g)) and SOA$_{MT\_OH(low\ NOx)}$ (16.1%, Fig.S17(e)). The different SOA$_{MT}$ components had regionally different or even opposite long-term trends. SOA$_{MT\_NO_3}$ showed a regionally consistent and significant increasing trend (Fig.S17(d)) in line with SOA$_{MT}$ (4.1% per decade) (Fig.7(e)). A slight but solid increasing trend in SOA$_{MT\_OH(high\ NOx)}$ is shown in Fig.S17(h), which together with the enhancement of SOA$_{MT\_NO_3}$ concentrations dominates the increasing trend in total SOA$_{MT}$. SOA$_{MT\_O_3}$ (Fig.S17(b)) and SOA$_{MT\_OH(low\ NOx)}$ (Fig.S17(f)) had similar trends but the change in SOA$_{MT\_OH(low\ NOx)}$ was relatively smaller.

370 The decreasing trend in $SOA_{MT\_O_3}$ and $SOA_{MT\_OH(low\ NOx)}$ offset the enhancement in the other two SOA_{MT} components. The different trends of SOA_{MT} components were affected by the changes in oxidants, which were mainly determined by changes in anthropogenic NOx emissions (Fig.8(b)). The mixing ratio of NOx and NO_3 increased over 1990-2019, while O_3 and OH increased relatively slowly, which led to differences in the variation of the SOA_{MT} components during the study period. The total SOA_{MT} has increased since 1990 primarily due to increased monoterpenes emissions because of higher temperature

375 (Fig.8(a)). Increased temperatures usually promote the BVOCs emissions (Guenther et al., 2012).
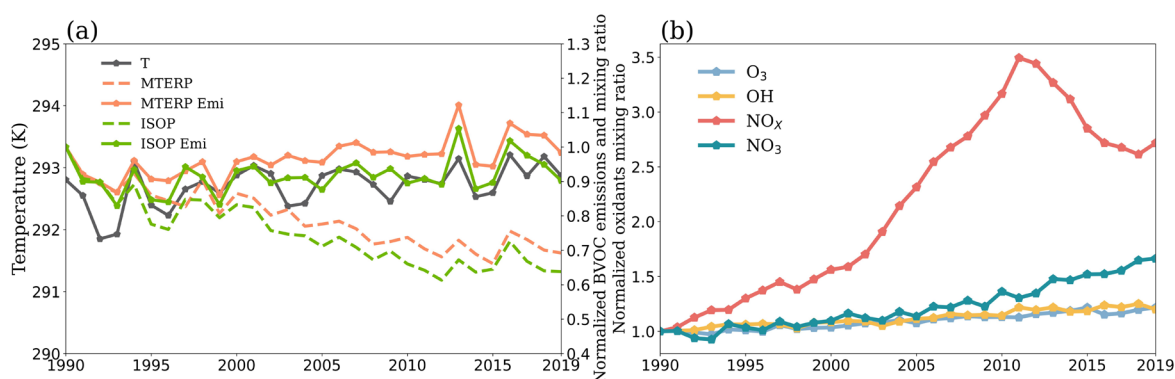
Figure 8: (a) 1990 to 2019 JJA time series of surface temperature (dark gray solid line; left Y axis; unit: K), normalized monoterpenes (orange dashed line; right Y axis) and isoprene (green dashed line; right Y axis) mixing ratios (MTERP and ISOP) and normalized
380 **surface monoterpenes (orange solid line; right Y axis) and isoprene (green solid line; right Y axis) emissions (MTERP Emi and ISOP Emi). (b) 1990 to 2019 JJA time series of surface normalized nitrogen oxidizes (NOx; red), ozone (O₃; pale blue), hydroxyl radical (OH; yellow), and nitrate radical (NO₃; cyan) mixing ratios. The ratio of the current year value to the 1990 value is used as the normalized value.**

385 Since anthropogenic NOx emission change may have a nonlinear effect on SOA_{MT}, we applied sensitivity simulations by perturbing NOx emissions and biogenic emissions respectively to quantify their contributions. We found that the response of SOA_{MT} to NOx emission change was almost negligible when NOx emissions rose to twice the 100nudging or fell to half the 100nudging in July 2013 (Fig.9(b)), although the major atmospheric oxidizers such as O_3, OH, NO_3, and NOx showed significant changes (Fig.S20). For example, the increase in NOx emissions drove $SOA_{MT\_OH(high\ NOx)}$ and $SOA_{MT\_OH(low\ NOx)}$ to

390 increase, but meanwhile, the effect was offset by decreases in $SOA_{MT\_NO_3}$ and $SOA_{MT\_O_3}$. Similarly, under condition of NOx emission reduction, the SOA_{MT} response was small due to the offsetting relative changes in the SOA_{MT} components. Our simulation results suggested that anthropogenic emission change has a very limited net effect on SOA_{MT} over the study period.

Through sensitivity simulations by perturbing monoterpenes emission, however, we found that the responses of SOA_{MT} and
395 its components were almost linear. When the monoterpenes emissions increased to twice that of the 100nudging in July 2013, the concentrations of SOA_{MT} and its components on the surface of China also increased by two times. Meanwhile, when the

monoterpenes emission decreased to half of the 100nudging, the concentrations of SOA$_{MT}$ and its components decreased by half too (Fig.9(a)). Changes in monoterpenes emissions showed a minor impact on atmospheric oxidants (Fig.S23). In brief summary, we found that anthropogenic NOx emission change has a very limited impact on SOA$_{MT}$, while enhanced

400 monoterpenes emissions due to a warmer surface temperature dominate the increasing trend over 1990-2019.
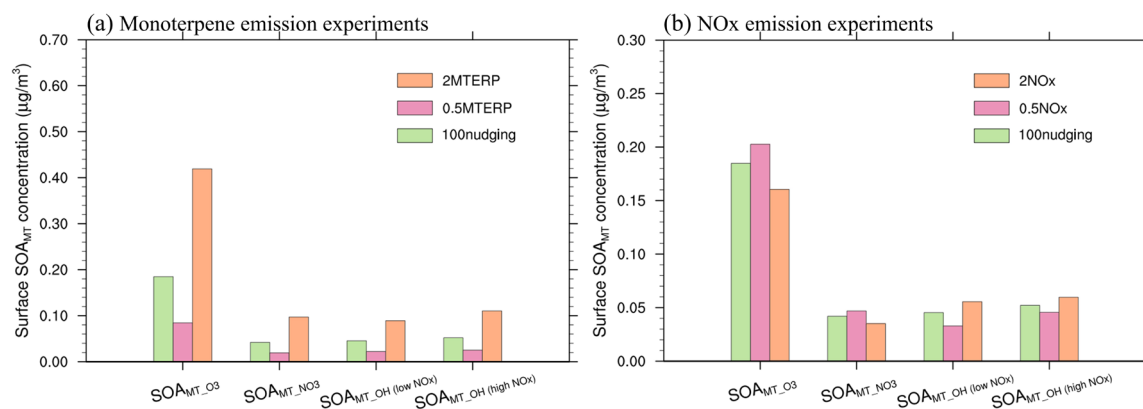
Figure 9: Surface concentrations (unit: μg m^{-3}) of monoterpene-derived secondary organic aerosols (SOA$_{MT}$) compositions for July 2013 from the monoterpenes (a) and NOx (b) sensitivity experiments named 100nudging (green bar), 0.5MTERP/NOx (pink bar),
405 **and 2MTERP/NOx (orange bar).**

4. Summary and discussion

In this study we applied the CAM-chem model along with ground-based measurements and the CAQRA-aerosols dataset to investigate the long-term trend of OA in 1990-2019 in China. A slight increase of total OA by 1.8% per decade was found to be a net effect of decrease in POA by -0.08 μg m^{-3} per decade (-2.7% per decade) and enhancement of SOA by 0.16 μg m^{-3}

410 per decade (10.8% per decade). There are significant regional differences in the change trend of OA, which generally decreased in the east (e.g., Yangtze River Delta) and increased in the west (e.g., Sichuan Basin), and this trend was more significant in winter, indicating the dominant contribution from primary anthropogenic emission of POA.

Further analyzing the causes of POA and SOA trends, we found that the main factors affecting POA trends are biomass burning
415 and anthropogenic emissions. Anthropogenic emissions accounted for 87.4% and dominated the long-term trend of POA, but biomass burning dominated the IAV. We found that anthropogenic VOCs made a major contribution to total SOA by 74.3% and the spatiotemporal characteristics were well consistent with POA. For SOA produced from BVOCs, we found in the simulation that BSOA plays an important role over South China especially in summer with contribution up to 47.1%. Total BSOA decreased by -4.1% over the study period. Isoprene derived SOA$_{IE}$ is greatly affected by heterogeneous reactions

420 catalyzed by sulfate, which decreased rapidly since 2006 and resulted in a decline by -18.8% over 1990-2019. On the other

hand, monoterpene-derived SOA$_{MT}$ increased by 12.3%. We found through sensitivity experiments that anthropogenic NOx emissions change had an almost negligible impact on total SOA$_{MT}$, although the contributions from different oxidation pathways changed slightly. The trend in SOA$_{MT}$ was dominated by increased biological emissions due to a warmer climate.

425 Our study revealed the change of total OA in China during the past 30 years and the contribution from various driving factors. Anthropogenic emission, biomass burning emission, and biogenic emission all showed important and unique impacts on the long-term trend of OA, indicating that future air quality management would be recommend to take a comprehensive consideration of the abovementioned sources. Especially, we found that anthropogenic contributions to both POA and SOA substantially decreased since 2014, while biogenic contribution has the potential to increase under a warming climate. BSOA

430 plays a minor role on a national scale but may have significant contribution over densely vegetated southern areas of China during summer, while a main part of it is hardly affected by anthropogenic emissions but is enhanced by a warming climate. This implies that future research may need to pay more attention to biogenic sources. In addition, it should be noticed that our current model may have deficiencies in terms of both emission inventory and chemical mechanism for simulating SOA. For example, current model only considers the heterogeneous production of IEPOX derived SOA, but recent studies show that

435 isoprene may also produce SOA through intermediate oxidation gas-phase products hydroxymethylmethyl-α-lactone (HMML) and methacrylic acid epoxide (MAE) (He et al., 2018; Zhang, 2023), which are not considered in the current model. This may also be partially responsible for the underestimation of SOA mentioned earlier. Therefore, continuous development of the SOA chemical mechanisms is recommended to improve the simulation capability of the model. And in addition, more detailed observations of OA components are needed to further investigate the interactions between biological and anthropogenic

440 sources.

Data availability. Ground-based measurements for OA, POA, and SOA were obtained from the supplementary materials of published articles by Miao et al. (2021) and Chen et al. (2024). The publicly available high-resolution simulation dataset of PM$_{2.5}$ composition over China (CAQRA-aerosols) was obtained from the Data Integration Project of the National Natural

445 Science Foundation's Air Pollution Complex Major Research Plan (Project Number: 92044303) via the China Air Pollution Data Center (CAPDC) (https://www.capdatabase.cn). The 24-hour average PM$_{2.5}$ and O$_3$ data can be accessed from the China Environmental Monitoring Terminal (CEMT) National Urban Air Quality Real-Time Distribution Platform (NUAQRDP) (https://air.cnemc.cn:18007/). MODIS AOD data is available at https://atmosphere-imager.gsfc.nasa.gov/products/aerosol. NO$_2$ column concentration data can be accessed from the OMI (Ozone Monitoring Instrument) Level-3 dataset on NASA's

450 AURA satellite platform (https://disc.gsfc.nasa.gov/datasets?keywords=OMI&page=1).

Author contributions. MW and XD designed the study. WZ performed the data analysis, produced the figures, and wrote the manuscript draft. YL and MY contributed to the model simulations. All the authors contributed to the discussion and editing of the manuscript.

455

Competing interests. At least one of the (co-)authors is a member of the editorial board of Atmospheric Chemistry and Physics.

Acknowledgments. This work is supported by the National Natural Science Foundation of China (grant numbers 41925023,

42075102), and the Fundamental Research Funds for the Central Universities - CEMAC "GeoX" Interdisciplinary Program

460 (2024ZD05) by the Frontiers Science Center for Critical Earth Material Cycling, Nanjing University. We greatly thank the

High Performance Computing Center (HPCC) of Nanjing University for providing the computational resources used in this

work. We also thank the Tsinghua University group for providing the MEIC emission used in our simulations. The CESM

project is supported primarily by the U.S. National Science Foundation.

References

465 An, Z., Huang, R.-J., Zhang, R., Tie, X., Li, G., Cao, J., Zhou, W., Shi, Z., Han, Y., Gu, Z., and Ji, Y.: Severe haze in northern China: A synergy of anthropogenic emissions and atmospheric processes, Proc. Natl. Acad. Sci., 116, 8657–8666, https://doi.org/10.1073/pnas.1900125116, 2019.

Cai, S., Wang, Y., Zhao, B., Wang, S., Chang, X., and Hao, J.: The impact of the "Air Pollution Prevention and Control Action Plan" on PM2.5 concentrations in Jing-Jin-Ji region during 2012–2020, Sci. Total Environ., 580, 197–209,

470 https://doi.org/10.1016/j.scitotenv.2016.11.188, 2017.

Chang, X., Zhao, B., Zheng, H., Wang, S., Cai, S., Guo, F., Gui, P., Huang, G., Wu, D., Han, L., Xing, J., Man, H., Hu, R., Liang, C., Xu, Q., Qiu, X., Ding, D., Liu, K., Han, R., Robinson, A. L., and Donahue, N. M.: Full-volatility emission framework corrects missing and underestimated secondary organic aerosol sources, One Earth, 5, 403–412, https://doi.org/10.1016/j.oneear.2022.03.015, 2022.

475 Chen, Q., Miao, R., Geng, G., Shrivastava, M., Dao, X., Xu, B., Sun, J., Zhang, X., Liu, M., Tang, G., Tang, Q., Hu, H., Huang, R.-J., Wang, H., Zheng, Y., Qin, Y., Guo, S., Hu, M., and Zhu, T.: Widespread 2013-2020 decreases and reduction challenges of organic aerosol in China, Nat. Commun., 15, 4465, https://doi.org/10.1038/s41467-024-48902-0, 2024.

Cui, L., Zhou, J., Peng, X., Ruan, S., and Zhang, Y.: Analyses of air pollution control measures and co-benefits in the heavily air-polluted Jinan city of China, 2013–2017, Sci. Rep., 10, 5423, https://doi.org/10.1038/s41598-020-62475-0, 2020.

480 Dalsøren, S. B., Isaksen, I. S. A., Li, L., and Richter, A.: Effect of emission changes in Southeast Asia on global hydroxyl and methane lifetime, Tellus B Chem. Phys. Meteorol., 61, 588, https://doi.org/10.1111/j.1600-0889.2009.00429.x, 2009.

Ding, X., Zhang, Y., He, Q., Yu, Q., Shen, R., Zhang, Y., Zhang, Z., Lyu, S., Hu, Q., Wang, Y., Li, L., Song, W., and Wang, X.: Spatial and seasonal variations of secondary organic aerosol from terpenoids over China, J. Geophys. Res. Atmospheres, 121, https://doi.org/10.1002/2016JD025467, 2016.

485 Donahue, N. M., Robinson, A. L., Stanier, C. O., and Pandis, S. N.: Coupled Partitioning, Dilution, and Chemical Aging of Semivolatile Organics, Environ. Sci. Technol., 40, 2635–2643, https://doi.org/10.1021/es052297c, 2006.

Dong, X., Liu, Y., Li, X., Yue, M., Liu, Y., Ma, Z., Zheng, H., Huang, R., and Wang, M.: Modeling Analysis of Biogenic Secondary Organic Aerosol Dependence on Anthropogenic Emissions in China, Environ. Sci. Technol. Lett., 9, 286–292, https://doi.org/10.1021/acs.estlett.2c00104, 2022.

490 Emmons, L. K., Schwantes, R. H., Orlando, J. J., Tyndall, G., Kinnison, D., Lamarque, J., Marsh, D., Mills, M. J., Tilmes, S., Bardeen, C., Buchholz, R. R., Conley, A., Gettelman, A., Garcia, R., Simpson, I., Blake, D. R., Meinardi, S., and Pétron, G.: The Chemistry Mechanism in the Community Earth System Model Version 2 (CESM2), J. Adv. Model. Earth Syst., 12, e2019MS001882, https://doi.org/10.1029/2019MS001882, 2020.

Fadel, M., Ledoux, F., Farhat, M., Kfoury, A., Courcot, D., and Afif, C.: PM2.5 characterization of primary and secondary

495 organic aerosols in two urban-industrial areas in the East Mediterranean, J. Environ. Sci., 101, 98–116, https://doi.org/10.1016/j.jes.2020.07.030, 2021.

Fan, Y., Liu, C.-Q., Li, L., Ren, L., Ren, H., Zhang, Z., Li, Q., Wang, S., Hu, W., Deng, J., Wu, L., Zhong, S., Zhao, Y., Pavuluri, C. M., Li, X., Pan, X., Sun, Y., Wang, Z., Kawamura, K., Shi, Z., and Fu, P.: Large contributions of biogenic and anthropogenic sources to fine organic aerosols in Tianjin, North China, Atmospheric Chem. Phys., 20, 117–137,

500 https://doi.org/10.5194/acp-20-117-2020, 2020.

Feng, Y., Ning, M., Lei, Y., Sun, Y., Liu, W., and Wang, J.: Defending blue sky in China: Effectiveness of the "Air Pollution Prevention and Control Action Plan" on air quality improvements from 2013 to 2017, J. Environ. Manage., 252, 109603, https://doi.org/10.1016/j.jenvman.2019.109603, 2019.

Gelaro, R., McCarty, W., Suárez, M. J., Todling, R., Molod, A., Takacs, L., Randles, C. A., Darmenov, A., Bosilovich, M. G.,

505 Reichle, R., Wargan, K., Coy, L., Cullather, R., Draper, C., Akella, S., Buchard, V., Conaty, A., Da Silva, A. M., Gu, W., Kim, G.-K., Koster, R., Lucchesi, R., Merkova, D., Nielsen, J. E., Partyka, G., Pawson, S., Putman, W., Rienecker, M., Schubert, S. D., Sienkiewicz, M., and Zhao, B.: The Modern-Era Retrospective Analysis for Research and Applications, Version 2 (MERRA-2), J. Clim., 30, 5419–5454, https://doi.org/10.1175/JCLI-D-16-0758.1, 2017.

Gettelman, A. and Morrison, H.: Advanced Two-Moment Bulk Microphysics for Global Models. Part I: Off-Line Tests and

510 Comparison with Other Schemes, J. Clim., 28, 1268–1287, https://doi.org/10.1175/JCLI-D-14-00102.1, 2015.

Grandey, B. S., Yeo, L. K., Lee, H., and Wang, C.: The Equilibrium Climate Response to Sulfur Dioxide and Carbonaceous Aerosol Emissions From East and Southeast Asia, Geophys. Res. Lett., 45, https://doi.org/10.1029/2018GL080127, 2018.

Guenther, A. B., Jiang, X., Heald, C. L., Sakulyanontvittaya, T., Duhl, T., Emmons, L. K., and Wang, X.: The Model of Emissions of Gases and Aerosols from Nature version 2.1 (MEGAN2.1): an extended and updated framework for modeling

515 biogenic emissions, Geosci. Model Dev., 5, 1471–1492, https://doi.org/10.5194/gmd-5-1471-2012, 2012.

Hallquist, M., Wenger, J. C., Baltensperger, U., Rudich, Y., Simpson, D., Claeys, M., Dommen, J., Donahue, N. M., George, C., Goldstein, A. H., Hamilton, J. F., Herrmann, H., Hoffmann, T., Iinuma, Y., Jang, M., Jenkin, M. E., Jimenez, J. L., Kiendler-Scharr, A., Maenhaut, W., McFiggans, G., Mentel, T. F., Monod, A., Prevot, A. S. H., Seinfeld, J. H., Surratt, J. D., Szmigielski, R., and Wildt, J.: The formation, properties and impact of secondary organic aerosol: current and emerging issues, Atmos

520 Chem Phys, 2009.

He, Q., Ding, X., Fu, X., Zhang, Y., Wang, J., Liu, Y., Tang, M., Wang, X., and Rudich, Y.: Secondary Organic Aerosol Formation From Isoprene Epoxides in the Pearl River Delta, South China: IEPOX- and HMML-Derived Tracers, J. Geophys. Res. Atmospheres, 123, 6999–7012, https://doi.org/10.1029/2017JD028242, 2018.

Hodzic, A., Kasibhatla, P. S., Jo, D. S., Cappa, C. D., Jimenez, J. L., Madronich, S., and Park, R. J.: Rethinking the global
525 secondary organic aerosol (SOA) budget: stronger production, faster removal, shorter lifetime, Atmospheric Chem. Phys., 16, 7917–7941, https://doi.org/10.5194/acp-16-7917-2016, 2016.

Hoyle, C. R., Boy, M., Donahue, N. M., Fry, J. L., Glasius, M., Guenther, A., Hallar, A. G., Huff Hartz, K., Petters, M. D., Petäjä, T., Rosenoern, T., and Sullivan, A. P.: A review of the anthropogenic influence on biogenic secondary organic aerosol, Atmospheric Chem. Phys., 11, 321–343, https://doi.org/10.5194/acp-11-321-2011, 2011.

530 Hu, J., Wang, P., Ying, Q., Zhang, H., Chen, J., Ge, X., Li, X., Jiang, J., Wang, S., Zhang, J., Zhao, Y., and Zhang, Y.: Modeling biogenic and anthropogenic secondary organic aerosol in China, Atmospheric Chem. Phys., 17, 77–92, https://doi.org/10.5194/acp-17-77-2017, 2017.

Hua, F., Wang, L., Fisher, B., Zheng, X., Wang, X., Yu, D. W., Tang, Y., Zhu, J., and Wilcove, D. S.: Tree plantations displacing native forests: The nature and drivers of apparent forest recovery on former croplands in Southwestern China from
535 2000 to 2015, Biol. Conserv., 222, 113–124, https://doi.org/10.1016/j.biocon.2018.03.034, 2018.

Huang, R.-J., Wang, Y., Cao, J., Lin, C., Duan, J., Chen, Q., Li, Y., Gu, Y., Yan, J., Xu, W., Fröhlich, R., Canonaco, F., Bozzetti, C., Ovadnevaite, J., Ceburnis, D., Canagaratna, M. R., Jayne, J., Worsnop, D. R., El-Haddad, I., Prévôt, A. S. H., and O'Dowd, C. D.: Primary emissions versus secondary formation of fine particulate matter in the most polluted city (Shijiazhuang) in North China, Atmospheric Chem. Phys., 19, 2283–2298, https://doi.org/10.5194/acp-19-2283-2019, 2019.

540 Jo, D. S., Hodzic, A., Emmons, L. K., Marais, E. A., Peng, Z., Nault, B. A., Hu, W., Campuzano-Jost, P., and Jimenez, J. L.: A simplified parameterization of isoprene-epoxydiol-derived secondary organic aerosol (IEPOX-SOA) for global chemistry and climate models: a case study with GEOS-Chem v11-02-rc, Geosci. Model Dev., 12, 2983–3000, https://doi.org/10.5194/gmd-12-2983-2019, 2019.

Jo, D. S., Hodzic, A., Emmons, L. K., Tilmes, S., Schwantes, R. H., Mills, M. J., Campuzano-Jost, P., Hu, W., Zaveri, R. A.,
545 Easter, R. C., Singh, B., Lu, Z., Schulz, C., Schneider, J., Shilling, J. E., Wisthaler, A., and Jimenez, J. L.: Future changes in isoprene-epoxydiol-derived secondary organic aerosol (IEPOX SOA) under the Shared Socioeconomic Pathways: the importance of physicochemical dependency, Atmospheric Chem. Phys., 21, 3395–3425, https://doi.org/10.5194/acp-21-3395-2021, 2021.

Kanellopoulos, P. G., Verouti, E., Chrysochou, E., Koukoulakis, K., and Bakeas, E.: Primary and secondary organic aerosol
550 in an urban/industrial site: Sources, health implications and the role of plastic enriched waste burning, J. Environ. Sci., 99, 222–238, https://doi.org/10.1016/j.jes.2020.06.012, 2021.

Kong, L., Tang, X., Zhu, J., Wang, Z., Li, J., Wu, H., Wu, Q., Chen, H., Zhu, L., Wang, W., Liu, B., Wang, Q., Chen, D., Pan, Y., Song, T., Li, F., Zheng, H., Jia, G., Lu, M., Wu, L., and Carmichael, G. R.: A 6-year-long (2013–2018) high-resolution air

quality reanalysis dataset in China based on the assimilation of surface observations from CNEMC, Earth Syst. Sci. Data, 13,
555   529–570, https://doi.org/10.5194/essd-13-529-2021, 2021.

Lee, S. C., Chiu, M. Y., Ho, K. F., Zou, S. C., and Wang, X.: Volatile organic compounds (VOCs) in urban atmosphere of
Hong Kong, Chemosphere, 48, 375–382, https://doi.org/10.1016/S0045-6535(02)00040-1, 2002.

Levy, R. C., Mattoo, S., Munchak, L. A., Remer, L. A., Sayer, A. M., Patadia, F., and Hsu, N. C.: The Collection 6 MODIS
aerosol products over land and ocean, Atmospheric Meas. Tech., 6, 2989–3034, https://doi.org/10.5194/amt-6-2989-2013,
560   2013.

Li, M., Liu, H., Geng, G., Hong, C., Liu, F., Song, Y., Tong, D., Zheng, B., Cui, H., Man, H., Zhang, Q., and He, K.:
Anthropogenic emission inventories in China: a review, Natl. Sci. Rev., 4, 834–866, https://doi.org/10.1093/nsr/nwx150, 2017.

Lin, C. Q., Liu, G., Lau, A. K. H., Li, Y., Li, C. C., Fung, J. C. H., and Lao, X. Q.: High-resolution satellite remote sensing of
provincial PM2.5 trends in China from 2001 to 2015, Atmos. Environ., 180, 110–116,
565   https://doi.org/10.1016/j.atmosenv.2018.02.045, 2018.

Liu, G., Ma, X., Li, W., Chen, J., Ji, Y., and An, T.: Pollution characteristics, source appointment and environmental effect of
oxygenated volatile organic compounds in Guangdong-Hong Kong-Macao Greater Bay Area: Implication for air quality
management, Sci. Total Environ., 919, 170836, https://doi.org/10.1016/j.scitotenv.2024.170836, 2024.

Liu, P., Zhou, H., Chun, X., Wan, Z., Liu, T., Sun, B., Wang, J., and Zhang, W.: Characteristics of fine carbonaceous aerosols
570   in Wuhai, a resource-based city in Northern China:Insights from energy efficiency and population density, Environ. Pollut.,
292, 118368, https://doi.org/10.1016/j.envpol.2021.118368, 2022.

Liu, X., Ma, P.-L., Wang, H., Tilmes, S., Singh, B., Easter, R. C., Ghan, S. J., and Rasch, P. J.: Description and evaluation of
a new four-mode version of the Modal Aerosol Module (MAM4) within version 5.3 of the Community Atmosphere Model,
Geosci. Model Dev., 9, 505–522, https://doi.org/10.5194/gmd-9-505-2016, 2016.

575   Liu, Y., Dong, X., Wang, M., Emmons, L. K., Liu, Y., Liang, Y., Li, X., and Shrivastava, M.: Analysis of secondary organic
aerosol simulation bias in the Community Earth System Model (CESM2.1), Atmospheric Chem. Phys., 21, 8003–8021,
https://doi.org/10.5194/acp-21-8003-2021, 2021a.

Liu, Y., Liu, Y., Wang, M., Dong, X., Zheng, Y., Shrivastava, M., Qian, Y., Bai, H., Li, X., and Yang, X.-Q.: Anthropogenic–
biogenic interaction amplifies warming from emission reduction over the southeastern US, Environ. Res. Lett., 16, 124046,
580   https://doi.org/10.1088/1748-9326/ac3285, 2021b.

Liu, Y., Dong, X., Emmons, L. K., Jo, D. S., Liu, Y., Shrivastava, M., Yue, M., Liang, Y., Song, Z., He, X., and Wang, M.:
Exploring the Factors Controlling the Long-Term Trend (1988–2019) of Surface Organic Aerosols in the Continental United
States by Simulations, J. Geophys. Res. Atmospheres, 128, e2022JD037935, https://doi.org/10.1029/2022JD037935, 2023.

Lu, X., Zhang, S., Xing, J., Wang, Y., Chen, W., Ding, D., Wu, Y., Wang, S., Duan, L., and Hao, J.: Progress of Air Pollution
585   Control in China and Its Challenges and Opportunities in the Ecological Civilization Era, Engineering, 6, 1423–1431,
https://doi.org/10.1016/j.eng.2020.03.014, 2020.

Ma, Z., Hu, X., Sayer, A. M., Levy, R., Zhang, Q., Xue, Y., Tong, S., Bi, J., Huang, L., and Liu, Y.: Satellite-Based Spatiotemporal Trends in PM $_{2.5}$ Concentrations: China, 2004–2013, Environ. Health Perspect., 124, 184–192, https://doi.org/10.1289/ehp.1409481, 2016.

590 Maji, K. J., Li, V. Ok., and Lam, J. Ck.: Effects of China's current Air Pollution Prevention and Control Action Plan on air pollution patterns, health risks and mortalities in Beijing 2014–2018, Chemosphere, 260, 127572, https://doi.org/10.1016/j.chemosphere.2020.127572, 2020.

Malm, W. C. and Hand, J. L.: An examination of the physical and optical properties of aerosols collected in the IMPROVE program, Atmos. Environ., 41, 3407–3427, https://doi.org/10.1016/j.atmosenv.2006.12.012, 2007.

595 Miao, R., Chen, Q., Shrivastava, M., Chen, Y., Zhang, L., Hu, J., Zheng, Y., and Liao, K.: Process-based and observation-constrained SOA simulations in China: the role of semivolatile and intermediate-volatility organic compounds and OH levels, Atmospheric Chem. Phys., 21, 16183–16201, https://doi.org/10.5194/acp-21-16183-2021, 2021.

Pye, H. O. T., Pinder, R. W., Piletic, I. R., Xie, Y., Capps, S. L., Lin, Y.-H., Surratt, J. D., Zhang, Z., Gold, A., Luecken, D. J., Hutzell, W. T., Jaoui, M., Offenberg, J. H., Kleindienst, T. E., Lewandowski, M., and Edney, E. O.: Epoxide Pathways

600 Improve Model Predictions of Isoprene Markers and Reveal Key Role of Acidity in Aerosol Formation, Environ. Sci. Technol., 47, 11056–11064, https://doi.org/10.1021/es402106h, 2013.

Pye, H. O. T., D'Ambro, E. L., Lee, B. H., Schobesberger, S., Takeuchi, M., Zhao, Y., Lopez-Hilfiker, F., Liu, J., Shilling, J. E., Xing, J., Mathur, R., Middlebrook, A. M., Liao, J., Welti, A., Graus, M., Warneke, C., De Gouw, J. A., Holloway, J. S., Ryerson, T. B., Pollack, I. B., and Thornton, J. A.: Anthropogenic enhancements to production of highly oxygenated molecules

605 from autoxidation, Proc. Natl. Acad. Sci., 116, 6641–6646, https://doi.org/10.1073/pnas.1810774116, 2019.

Qin, M., Wang, X., Hu, Y., Ding, X., Song, Y., Li, M., Vasilakos, P., Nenes, A., and Russell, A. G.: Simulating Biogenic Secondary Organic Aerosol During Summertime in China, J. Geophys. Res. Atmospheres, 123, https://doi.org/10.1029/2018JD029185, 2018.

Schwantes, R. H., Emmons, L. K., Orlando, J. J., Barth, M. C., Tyndall, G. S., Hall, S. R., Ullmann, K., St. Clair, J. M., Blake,

610 D. R., Wisthaler, A., and Bui, T. P. V.: Comprehensive isoprene and terpene gas-phase chemistry improves simulated surface ozone in the southeastern US, Atmospheric Chem. Phys., 20, 3739–3776, https://doi.org/10.5194/acp-20-3739-2020, 2020.

Shilling, J. E., Zaveri, R. A., Fast, J. D., Kleinman, L., Alexander, M. L., Canagaratna, M. R., Fortner, E., Hubbe, J. M., Jayne, J. T., Sedlacek, A., Setyan, A., Springston, S., Worsnop, D. R., and Zhang, Q.: Enhanced SOA formation from mixed anthropogenic and biogenic emissions during the CARES campaign, Atmospheric Chem. Phys., 13, 2091–2113,

615 https://doi.org/10.5194/acp-13-2091-2013, 2013.

Shrivastava, M., Cappa, C. D., Fan, J., Goldstein, A. H., Guenther, A. B., Jimenez, J. L., Kuang, C., Laskin, A., Martin, S. T., Ng, N. L., Petaja, T., Pierce, J. R., Rasch, P. J., Roldin, P., Seinfeld, J. H., Shilling, J., Smith, J. N., Thornton, J. A., Volkamer, R., Wang, J., Worsnop, D. R., Zaveri, R. A., Zelenyuk, A., and Zhang, Q.: Recent advances in understanding secondary organic aerosol: Implications for global climate forcing, Rev. Geophys., 55, 509–559, https://doi.org/10.1002/2016RG000540, 2017.

620 Shrivastava, M., Andreae, M. O., Artaxo, P., Barbosa, H. M. J., Berg, L. K., Brito, J., Ching, J., Easter, R. C., Fan, J., Fast, J. D., Feng, Z., Fuentes, J. D., Glasius, M., Goldstein, A. H., Alves, E. G., Gomes, H., Gu, D., Guenther, A., Jathar, S. H., Kim, S., Liu, Y., Lou, S., Martin, S. T., McNeill, V. F., Medeiros, A., De Sá, S. S., Shilling, J. E., Springston, S. R., Souza, R. A. F., Thornton, J. A., Isaacman-VanWertz, G., Yee, L. D., Ynoue, R., Zaveri, R. A., Zelenyuk, A., and Zhao, C.: Urban pollution greatly enhances formation of natural aerosols over the Amazon rainforest, Nat. Commun., 10, 1046,
625 https://doi.org/10.1038/s41467-019-08909-4, 2019.

Tilmes, S., Hodzic, A., Emmons, L. K., Mills, M. J., Gettelman, A., Kinnison, D. E., Park, M., Lamarque, J. -F., Vitt, F., Shrivastava, M., Campuzano-Jost, P., Jimenez, J. L., and Liu, X.: Climate Forcing and Trends of Organic Aerosols in the Community Earth System Model (CESM2), J. Adv. Model. Earth Syst., 11, 4323–4351, https://doi.org/10.1029/2019MS001827, 2019.

630 Tong, D., Cheng, J., Liu, Y., Yu, S., Yan, L., Hong, C., Qin, Y., Zhao, H., Zheng, Y., Geng, G., Li, M., Liu, F., Zhang, Y., Zheng, B., Clarke, L., and Zhang, Q.: Dynamic projection of anthropogenic emissions in China: methodology and 2015–2050 emission pathways under a range of socio-economic, climate policy, and pollution control scenarios, Atmospheric Chem. Phys., 20, 5729–5757, https://doi.org/10.5194/acp-20-5729-2020, 2020.

Wang, L., Jin, X., Wang, Q., Mao, H., Liu, Q., Weng, G., and Wang, Y.: Spatial and temporal variability of open biomass
635 burning in Northeast China from 2003 to 2017, Atmospheric Ocean. Sci. Lett., 13, 240–247, https://doi.org/10.1080/16742834.2020.1742574, 2020.

Xing, L., Fu, T.-M., Liu, T., Qin, Y., Zhou, L., Chan, C. K., Guo, H., Yao, D., and Duan, K.: Estimating organic aerosol emissions from cooking in winter over the Pearl River Delta region, China, Environ. Pollut., 292, 118266, https://doi.org/10.1016/j.envpol.2021.118266, 2022.

640 Xu, B., Wang, T., Ma, D., Song, R., Zhang, M., Gao, L., Li, S., Zhuang, B., Li, M., and Xie, M.: Impacts of regional emission reduction and global climate change on air quality and temperature to attain carbon neutrality in China, Atmospheric Res., 279, 106384, https://doi.org/10.1016/j.atmosres.2022.106384, 2022.

Xu, Z. N., Nie, W., Liu, Y. L., Sun, P., Huang, D. D., Yan, C., Krechmer, J., Ye, P. L., Xu, Z., Qi, X. M., Zhu, C. J., Li, Y. Y., Wang, T. Y., Wang, L., Huang, X., Tang, R. Z., Guo, S., Xiu, G. L., Fu, Q. Y., Worsnop, D., Chi, X. G., and Ding, A. J.:
645 Multifunctional Products of Isoprene Oxidation in Polluted Atmosphere and Their Contribution to SOA, Geophys. Res. Lett., 48, e2020GL089276, https://doi.org/10.1029/2020GL089276, 2021.

Yue, M., Dong, X., Wang, M., Emmons, L. K., Liang, Y., Tong, D., Liu, Y., and Liu, Y.: Modeling the Air Pollution and Aerosol-PBL Interactions Over China Using a Variable-Resolution Global Model, J. Geophys. Res. Atmospheres, 128, e2023JD039130, https://doi.org/10.1029/2023JD039130, 2023.

650 Zaveri, R. A., Easter, R. C., Fast, J. D., and Peters, L. K.: Model for Simulating Aerosol Interactions and Chemistry (MOSAIC), J. Geophys. Res. Atmospheres, 113, 2007JD008782, https://doi.org/10.1029/2007JD008782, 2008.

Zaveri, R. A., Easter, R. C., Singh, B., Wang, H., Lu, Z., Tilmes, S., Emmons, L. K., Vitt, F., Zhang, R., Liu, X., Ghan, S. J., and Rasch, P. J.: Development and Evaluation of Chemistry-Aerosol-Climate Model CAM5-Chem-MAM7-MOSAIC: Global

Atmospheric Distribution and Radiative Effects of Nitrate Aerosol, J. Adv. Model. Earth Syst., 13, e2020MS002346,

655 https://doi.org/10.1029/2020MS002346, 2021.

Zhang, G. J. and McFarlane, N. A.: Sensitivity of climate simulations to the parameterization of cumulus convection in the Canadian climate centre general circulation model, Atmosphere-Ocean, 33, 407–446, https://doi.org/10.1080/07055900.1995.9649539, 1995.

Zhang, H., Yee, L. D., Lee, B. H., Curtis, M. P., Worton, D. R., Isaacman-VanWertz, G., Offenberg, J. H., Lewandowski, M.,

660 Kleindienst, T. E., Beaver, M. R., Holder, A. L., Lonneman, W. A., Docherty, K. S., Jaoui, M., Pye, H. O. T., Hu, W., Day, D. A., Campuzano-Jost, P., Jimenez, J. L., Guo, H., Weber, R. J., De Gouw, J., Koss, A. R., Edgerton, E. S., Brune, W., Mohr, C., Lopez-Hilfiker, F. D., Lutz, A., Kreisberg, N. M., Spielman, S. R., Hering, S. V., Wilson, K. R., Thornton, J. A., and Goldstein, A. H.: Monoterpenes are the largest source of summertime organic aerosol in the southeastern United States, Proc. Natl. Acad. Sci., 115, 2038–2043, https://doi.org/10.1073/pnas.1717513115, 2018.

665 Zhang, J.: New formation and fate of Isoprene SOA markers revealed by field data-constrained modeling, 2023.

Zhang, Q., Jimenez, J. L., Canagaratna, M. R., Allan, J. D., Coe, H., Ulbrich, I., Alfarra, M. R., Takami, A., Middlebrook, A. M., Sun, Y. L., Dzepina, K., Dunlea, E., Docherty, K., DeCarlo, P. F., Salcedo, D., Onasch, T., Jayne, J. T., Miyoshi, T., Shimono, A., Hatakeyama, S., Takegawa, N., Kondo, Y., Schneider, J., Drewnick, F., Borrmann, S., Weimer, S., Demerjian, K., Williams, P., Bower, K., Bahreini, R., Cottrell, L., Griffin, R. J., Rautiainen, J., Sun, J. Y., Zhang, Y. M., and Worsnop, D.

670 R.: Ubiquity and dominance of oxygenated species in organic aerosols in anthropogenically-influenced Northern Hemisphere midlatitudes, Geophys. Res. Lett., 34, 2007GL029979, https://doi.org/10.1029/2007GL029979, 2007.

Zheng, B., Tong, D., Li, M., Liu, F., Hong, C., Geng, G., Li, H., Li, X., Peng, L., Qi, J., Yan, L., Zhang, Y., Zhao, H., Zheng, Y., He, K., and Zhang, Q.: Trends in China's anthropogenic emissions since 2010 as the consequence of clean air actions, Atmospheric Chem. Phys., 18, 14095–14111, https://doi.org/10.5194/acp-18-14095-2018, 2018.

675 Zheng, H., Chang, X., Wang, S., Li, S., Zhao, B., Dong, Z., Ding, D., Jiang, Y., Huang, G., Huang, C., An, J., Zhou, M., Qiao, L., and Xing, J.: Sources of Organic Aerosol in China from 2005 to 2019: A Modeling Analysis, Environ. Sci. Technol., 57, 5957–5966, https://doi.org/10.1021/acs.est.2c08315, 2023a.

Zheng, H., Chang, X., Wang, S., Li, S., Yin, D., Zhao, B., Huang, G., Huang, L., Jiang, Y., Dong, Z., He, Y., Huang, C., and Xing, J.: Trends of Full-Volatility Organic Emissions in China from 2005 to 2019 and Their Organic Aerosol Formation

680 Potentials, Environ. Sci. Technol. Lett., 10, 137–144, https://doi.org/10.1021/acs.estlett.2c00944, 2023b.

Zheng, Y., Miao, R., Zhang, Q., Li, Y., Cheng, X., Liao, K., Koenig, T. K., Ge, Y., Tang, L., Shang, D., Hu, M., Chen, S., and Chen, Q.: Secondary Formation of Submicron and Supermicron Organic and Inorganic Aerosols in a Highly Polluted Urban Area, J. Geophys. Res. Atmospheres, 128, e2022JD037865, https://doi.org/10.1029/2022JD037865, 2023c.

Zhong, Y., Chen, J., Zhao, Q., Zhang, N., Feng, J., and Fu, Q.: Temporal trends of the concentration and sources of secondary

685 organic aerosols in PM$_{2.5}$ in Shanghai during 2012 and 2018, Atmos. Environ., 261, 118596, https://doi.org/10.1016/j.atmosenv.2021.118596, 2021.

Zhuang, Y., Li, R., Yang, H., Chen, D., Chen, Z., Gao, B., and He, B.: Understanding Temporal and Spatial Distribution of Crop Residue Burning in China from 2003 to 2017 Using MODIS Data, Remote Sens., 10, 390, https://doi.org/10.3390/rs10030390, 2018.

690